Insights Into the Acoustic Near and Far Field Based on Synchronized PIV and Microphone Measurements

Lars Siegel[1], **Arne Henning**[*1], **Klaus Ehrenfried**[1], **Claus Wagner**[1,2]

1: German Aerospace Center (DLR), Institute for Aerodynamics and Flow Technology, Göttingen, Germany
2: Technical University Ilmenau, Institute of Thermodynamics and Fluid Mechanics, Ilmenau, Germany
*corresponding author: arne.henning@dlr.de

Keywords: Aeroacoustics, PIV, Causality Correlation

Abstract

The aim of this study is to detect and visualize the propagating sound waves emanating from a flow around different types of rods. For this purpose, synchronous Particle Image Velocimetry (PIV) and microphone measurements were performed in an aeroacoustic wind tunnel. The velocity fluctuations were recorded not only in the vicinity of the rods but also in several regions between the wake flow field and the far field microphone. By means of the correlation between velocity and pressure fluctuations, coherent structures within and outside the flow could be identified. In particular, the temporal and spatial development of these structures provides an insight into the sound generation mechanism and the transition between the acoustic near and far field. The results are compared with analytical and numerical solutions.

1. Introduction

The localization of the sound sources generated by turbulent flows is one of the major tasks in the field of aeroacoustics. While great progress has already been made in the development of numerical and experimental methods for quantifying fluctuations in turbulent flows, the calculation of the effectively emitted sound remains a major challenge [8]. The reason for this is the disparity between the pressure fluctuations in the turbulent region and the extremely small part which is radiated into the far field. Thus, a numerical or experimental method must have a high resolution and accuracy, so that the small proportions still resolve.

On the other hand, there are well known generic flow configurations like the cylinder wake, which allow for good predictions in terms of the frequency distribution and strength of the sound radiation [16, 17, 9]. In the past it was shown that aeroacoustic sources can be identified by synchronous velocity measurements using PIV in the turbulent flow region and by means of pressure measurements with microphones in the acoustic far field. Analyzing the cross-correlation function between the two variables enables the identification of flow structures which are part of the noise-generating process [7, 12, 13]. In all previous works, in which this so-called causality correlation technique was used, the focus was on capturing the flow structures in the near field of the flow [1, 2, 3]. However, the results have already shown that significant coefficients can also be measured in areas outside the turbulent flow region [2]. These observations already emphasize the fact that in most cases, areas where the fluctuations of the flow correlate with the pressure in the far field, cannot be interpreted simply as a source of sound generation. One focus of the work presented here is therefore the investigation of the correlation between the pressure fluctuations in the far field and the velocity fluctuations in the entire area between the position of the body exposed to the flow and the position of the microphone. The aim is to gain knowledge about the transition of the fluid mechanic fluctuations in the near field of the flow and the acoustic fluctuations in the acoustic far field. The measurements were carried out on different rod and cylinder configurations. Here, mainly the results of a square-rod configuration are shown. For a deeper understanding of the correlation results, results of an analytical and a numerical calculation were compared with the experimental results.

2. Correlation Function

The sample cross-correlation function $S_{p,\Psi}(\mathbf{x}, \tau)$ is defined as:

$$S_{p,\Psi}(\mathbf{x}, \mathbf{y}, \tau) = \frac{1}{N} \sum_{i=1}^{N} \Psi'(\mathbf{x}, t_i) p'(\mathbf{y}, t_i + \tau), \tag{1}$$

where $\Psi'(\mathbf{x}, \tau)$ represents the zero-mean part of a near-field quantity measured at position $\mathbf{x}$ and time t_i, $p(\mathbf{y}, t_i + \tau)$ is the pressure fluctuation at position $\mathbf{y}$ at time $t_i + \tau$, with τ representing the differences between the points in time when the pressure and flow quantity are recorded. N is the number of samples of Ψ ($N = 15000$ in the present case). The cross-correlation function can be regarded as a result from a filtering process for the near-field fluctuations, extracting the parts showing a linear dependency with the far-field pressure fluctuations. Thus, the velocity fluctuations filtered in this way can be used as a proxy variable for the acoustic particle velocity.

In order to make the experimental results comparable to the analytical and numerical solution, the correlation function is scaled in the following manner:

$$L_s = \underbrace{sgn(S_{p,\Psi}) \cdot log\left(\frac{|S_{p,\Psi}|}{c_0 \cdot p_0}\right)}_{L_s^*} / max(|L_s^*|), \tag{2}$$

with c_0 being the speed of sound and p_0 representing the ambient pressure. Accordingly, the numerical and analytical solutions are scaled as follows:

$$L_v = \underbrace{sgn(v') \cdot log\left(\frac{|v'|}{v_0}\right)}_{L_v^*} / max(|L_v^*|), \tag{3}$$

with v' being the acoustic particle velocity resulting from the numerical and analytical solution, respectively and $v_0 = 5 \cdot 10^{-8}$m/s representing a reference particle velocity in air.

3. Numerical Simulation and Analytical Solution of a Moving Dipole

For a deeper understanding of the correlation results, a 2D simulation of a moving acoustic dipole was carried out. The open source *k-wave* toolbox was used to solve the coupled differential equations of first order (Euler's equation, conservation of mass and pressure-density relation) [14]. To solve the equations, a k-space-pseudo-spectral method was used, in which a Fourier collocation scheme was applied to calculate the spatial gradients [15]. The tem-

poral gradients were calculated with a finite difference scheme corrected for k-space. In addition, the toolbox was equipped with a Perfect Matched Layer (PML) which ensures anechoic conditions at the boundaries of the computational domain. In order to simulate the flow around the rod, the source was moved to simulate the case considered here, which corresponds to the flow around the source. The speed of the movement was adjusted to the speed of the wind tunnel in order to make it comparable with the flow around the selected rod. Assuming that the acoustic radiation of a rod in a flow corresponds to a dipole and implementing the simplification of perfect spanwise coherence, the simulation was carried out in 2D and with a dipole as source. The amplitude, wavelength and frequency of the source as well as the temporal resolution of the simulation were selected in accordance with the measured values used in the experiment. The size of the computational domain was designed in such a way that the movement of the source could be resolved over several periods of the oscillating dipole and all observed PIV fields of view are covered. The movement of the source begins after the initial acoustic propagation has reached the limits of the simulation domain. For the sake of simplicity and as a first starting point, the source was treated as a point source, neglecting the finite dimensions of the rod.

For the analytical solution, the assumptions were consistent with the numerical solution described in the previous section, namely, that the source is a dipole which can be represented in a 2D domain. The convected wave equation was solved using a Green's function, resulting in an analytical expression for the acoustic particle velocity of a mass or heat source in uniform flow for the 2D case. For the present case, two sources were implemented in a distance equal to the rod diameter and with opposite phase to realize a dipole.

4. Experimental Setup

The experiments were conducted in the Aeroacoustic Wind Tunnel Braunschweig (AWB) of the German Aerospace Center (DLR). The AWB is a Göttingen-type wind tunnel with an open test section and a rectangular nozzle outlet of $0.8\,\mathrm{m} \times 1.2\,\mathrm{m}$ [10]. The wind tunnel is optimized for aeroacoustic measurements and has an anechoic plenum. Figure 1 shows a

schematic view and an image of the experimental setup. Measurements were carried out at a free-stream velocity of $U_\infty = 60\,\mathrm{m/s}$. Different kinds of cylindrical and square rods were mounted between two end plates which extended the lateral walls of the nozzle exit. The span was $s = 0.8\,\mathrm{m}$ with a cross section of $15 \times 15\,\mathrm{mm}^2$ in case of the square rods and a diameter of $15\,\mathrm{mm}$ in case of the cylinder. The rods were equipped with a pressure sensor (type: 8507C-; Endevco) positioned on the half span to measure the lee-side pressure fluctuations. The side windows were equipped with borosilicate glass inserts to provide visual access for PIV.

The two components of the flow velocity in the plane perpendicular to the rods were measured by means of a PIV system (2D2C-PIV [11]) in different regions of interest (ROI) in the area between the respective rod and the microphone positions. DEHS particles with an average diameter of $1\mu m$ were introduced into the flow [5, 6]. They were illuminated by means of a double-pulsed laser (Nd: YAG; type: Innolas Spitlight 600) with a maximum energy of $350\,\mathrm{mJ}$ per pulse, equipped with light sheet optics. The frequency of the double pulses was $14\,\mathrm{Hz}$. The particle images were taken with a CMOS camera (PCO edge 5.5) with a resolution of $2560\,\mathrm{px} \times 2160\,\mathrm{px}$ and a frame rate of $14\,\mathrm{Hz}$ in direct-to-disc storage mode. 15000 double images were recorded for each ROI. The entire PIV system was mounted on a vertically traversing table in order to allow a quick change between the different ROI. The resolution of the measurement was $23.1\,\mathrm{px/mm}$. The pressure measurements in the far field were carried out with four microphones (type: 1/2 40 AC; G. R. A. S.) arranged in a horizontal line parallel to the free stream above the rod outside the flow. The vertical distance from the mics to the rod was $66.6\,\mathrm{d}$. A multi-analyser (type: OR36; OROS) simultaneously recorded the microphone, camera and pressure sensor signals with a sampling frequency of $f_s = 51.2\,\mathrm{kHz}$ and a dynamic range of $24\,\mathrm{bits}$. All channels had an anti-aliasing filter at $f_u = 25.6\,\mathrm{kHz}$. In order to reduce the influence of low-frequency wind tunnel noise on the measurement signals, a high-pass filter with a cut-off frequency $f_l = 200\,\mathrm{Hz}$ was used. The PIV measurements were performed synchronously with the microphone recordings. In ROI A and F, the dynamic range of the PIV was approx. $46\,\mathrm{dB}$ to dissolve the vortex structure in

the wake of the rod. In the ROI B to E, much higher dynamic ranges were achieved (ROI C: ≈ 72 dB) in order to resolve the acoustic fluctuations in the far field.

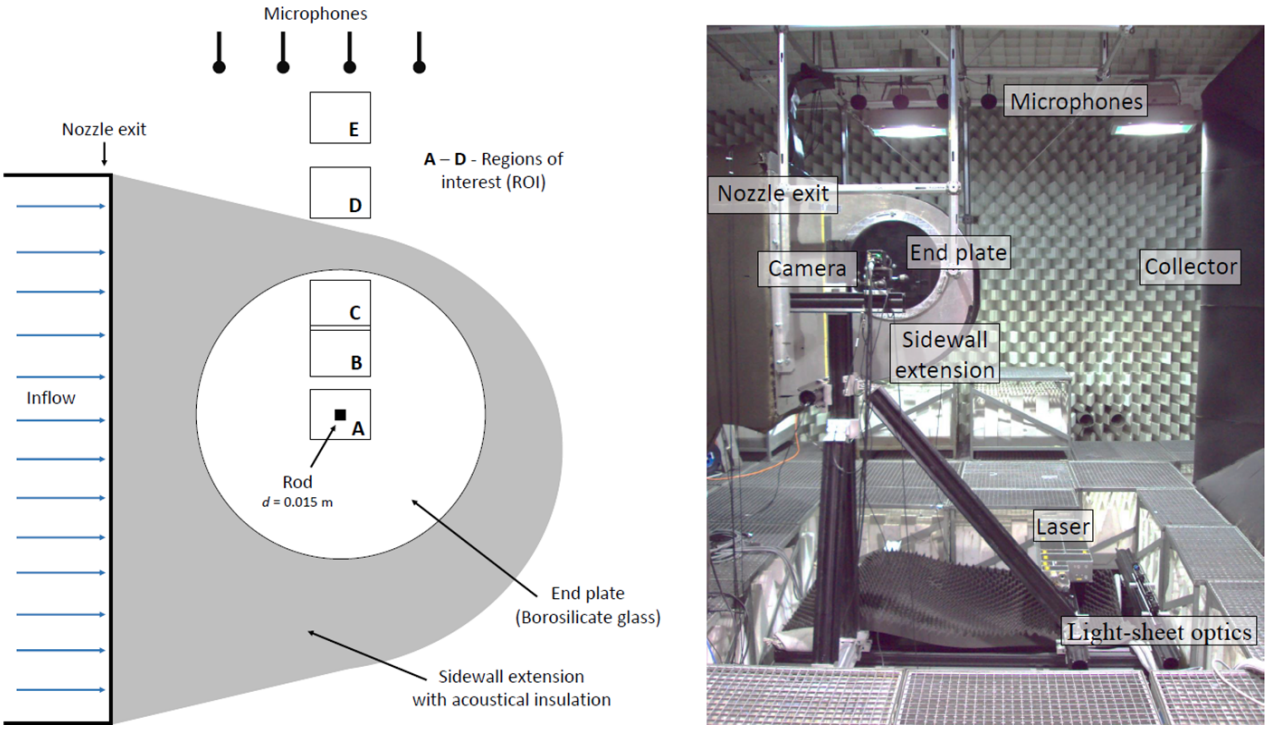

Figure 1: *Left:* Schematic view of the experimental setup. *Right:* Image of the experimental setup.

5. Results and Discussion

The axes in the following figures are scaled to the characteristic length scale of the rod $d = 15\,\text{mm}$. x and y are right-handed Cartesian coordinates with the origin at the center of the square rod. The values u and v are the velocity components in the x and y direction, respectively. In case of the 2D simulation, the source moves from the right to the left. Only results for the square rod are shown, featuring the highest absolute sound pressure level and, therefore, the radiated acoustic perturbations are most significant in this case. Only the PIV ROI A, B, C, D and E are considered in the following discussion. The model contours are depicted in black and grey whereas the white areas indicate the masking of the PIV processing and the gaps between the fields of view. Please note that mainly the velocity component v pointing in the direction of the chosen microphone is considered. This is the

main direction of the sound radiation produced by the flow around the rod.

Figure 2 shows the frequency distribution of the pressure signal recorded with the microphone (third microphone from the left in figure 1) directly above the installed square rod. The dominant peak at $f_p = 515.6\,\text{Hz}$ corresponds to a *Strouhal*-number of $St = (f_p d)/U_\infty = 0.129$. Figure 3 shows the mean and standard deviation of the vertical velocity component v.

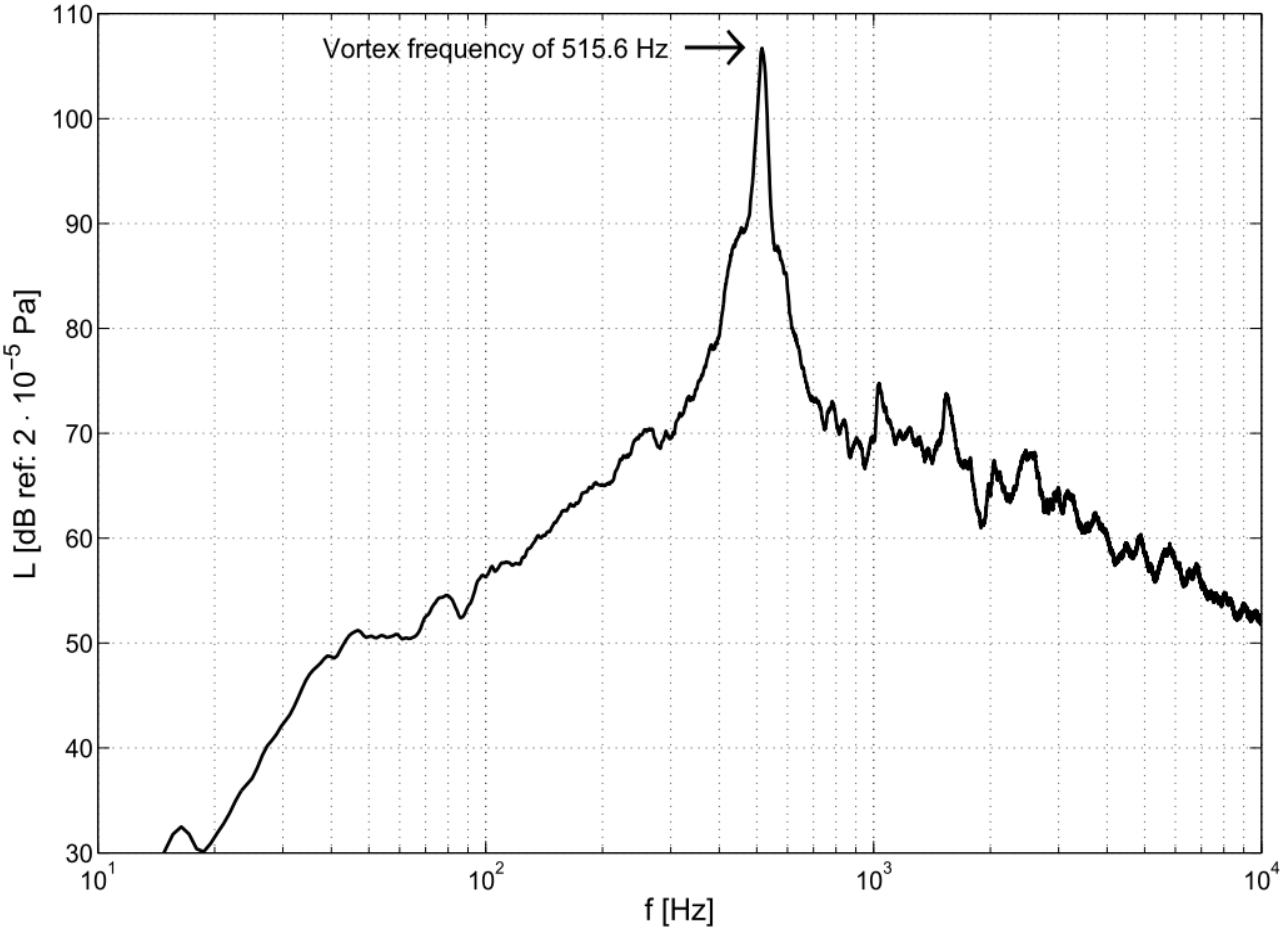

Figure 2: Frequency spectra of the far-field pressure fluctuations in case of the square rod.

The values show the typical spatial distribution as it is to be expected at a *von Kármán* vortex street downstream of the rod. The vortices emanating from both sides of the rod with alternating orientation produce a structure which rolls from both sides of the rod to line $y = 0$, resulting in maximum absolute values of v in the vicinity of the downstream corners of the rod. A region of low mean values and fluctuations can be observed in the typical dead water zone on the leeward side of the rod. The alternating orientation of the evolving vortices

results in a maximal standard deviation of about $x/d = 1.6$, a value which corresponds well with the findings in the literature [4]. Figure 4 depicts the instantaneous distributions of

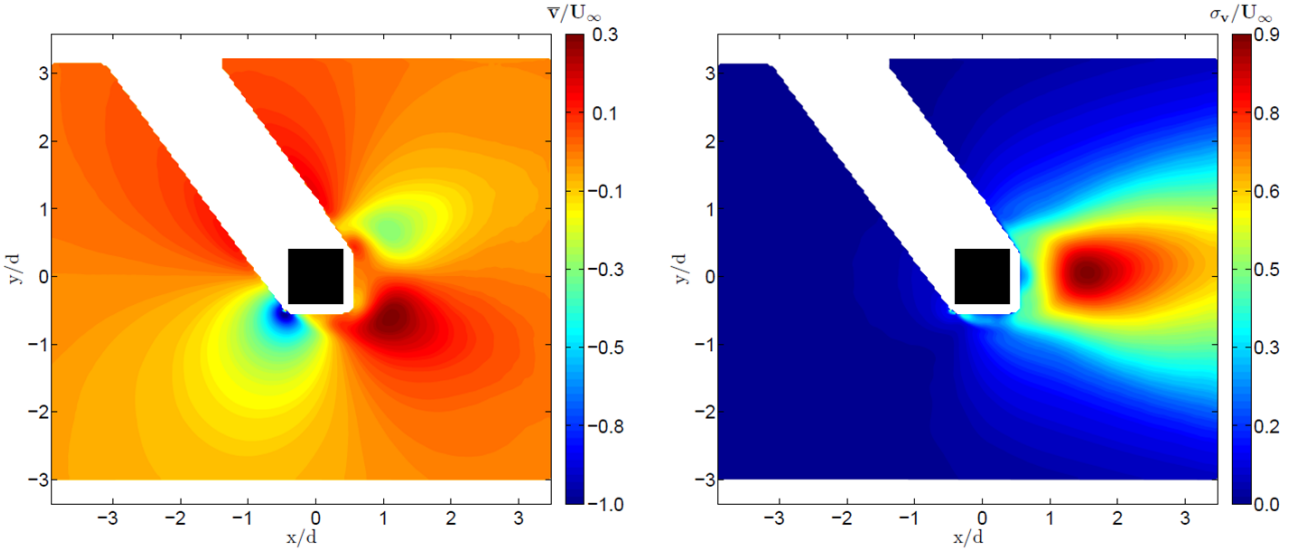

Figure 3: *Left:* mean vertical velocity distribution in the vicinity of the rod; *Right:* standard deviation of the vertical velocity component v in the vicinity of the rod.

the cross-correlation function L_s for $\Psi = v$ for different time differences τ between the PIV and the microphone measurement. Close to the rod, the topology of the correlation function agrees with findings in the literature [1]. Regions with high values of L_s with alternating sign are convecting along the axis $y = 0$ with increasing τ. It has been shown previously, that in case of a *von Kármán* vortex street, the phase shift of the correlation function along the main trajectory, corresponds to the average velocity of the large-scale vortices emanating from the rod further downstream [2]. The distance between maximum correlation values along $y = 0$ corresponds to the averaged distance of these large-scale vortices. Assuming that the correlation function behaves like a filter for the acoustic fluctuations, the correlation function can be considered as a qualitative examination of the acoustic particle velocity in the region outside the wake of the rod. If so, the spatial distribution of the correlation with varying τ in the areas outside the turbulent flow, reflects the wave propagation from the rod towards the microphone quit well. The homogeneous distribution is disturbed in the area of the shear layer ($28 < y/d <$34) located at the transition between the free jet of the wind tunnel nozzle and the air at rest in the plenum. In order to compare the results of the

measurements with those of the numerical and analytical solution, the respective results are shown in Figure 5 for selected points in time. The vertical line marks an area which is considered in a later analysis. The comparison shows that the cross-correlation function reflects wave propagation in a similar way as the acoustic particle velocity. Since the analytical solution does not contain the generation of vortices, the largest deviations in the area of the rod can be observed here.

6. Conclusion

It is shown that the generation and propagation of the acoustic particle velocity can be successfully investigated by synchronous velocity measurements in- and outside the flow field via PIV and pressure recordings in the far field. The cross-correlation function between these two variables then serves as a proxy variable for the acoustic particle velocity. The acoustic wave propagation of a strong tonal source generated by a uniform flow around a square rod can be resolved and reproduced in the vicinity of the source through the wind tunnel shear layer into the acoustic far field. The validity of the approach has been proven by comparing it with the 2D simulation and a 2D analysis solution. Results presented here show good agreement for all three cases.

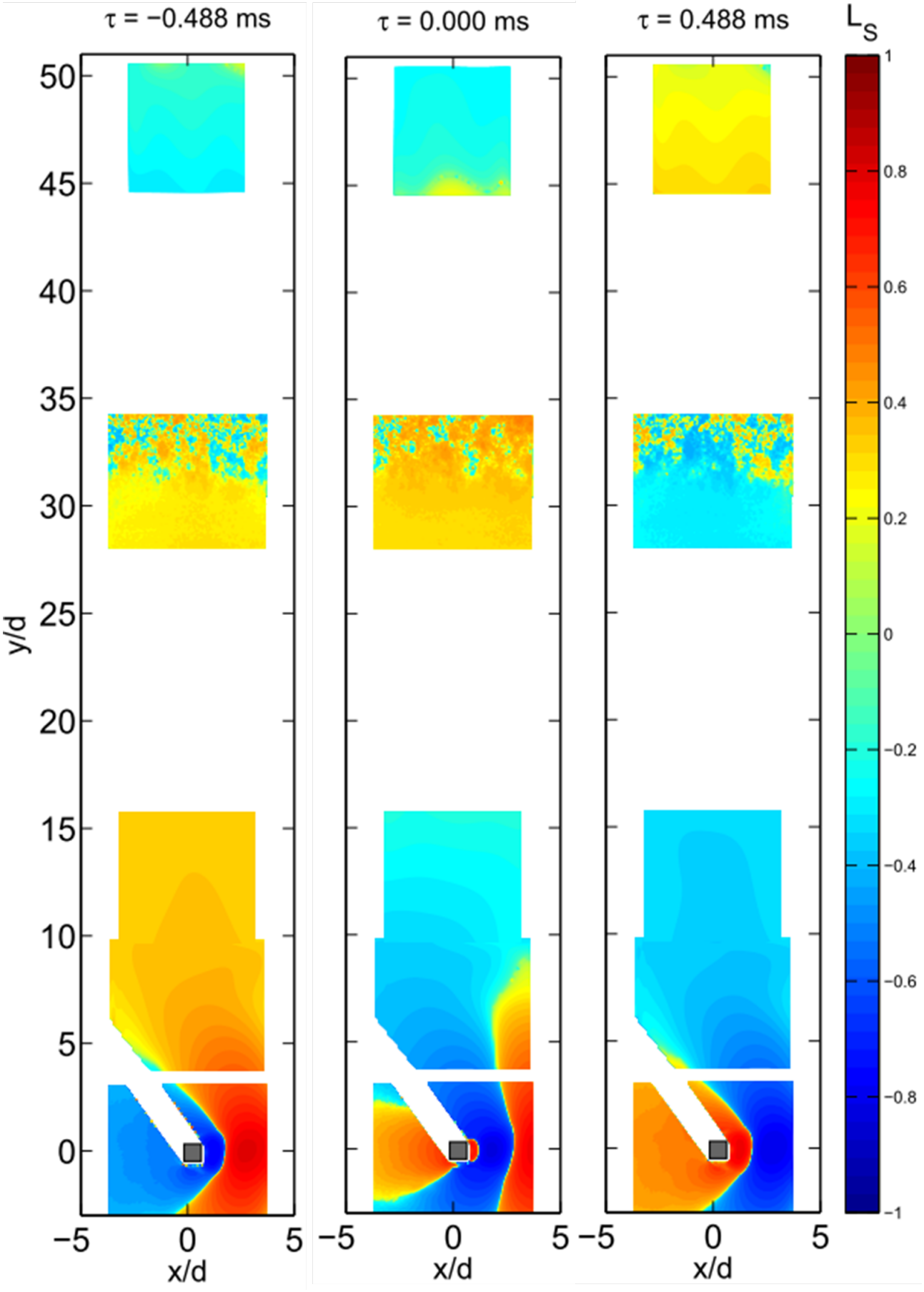

Figure 4: Instantaneous distributions of the cross-correlation function for different points in time τ.

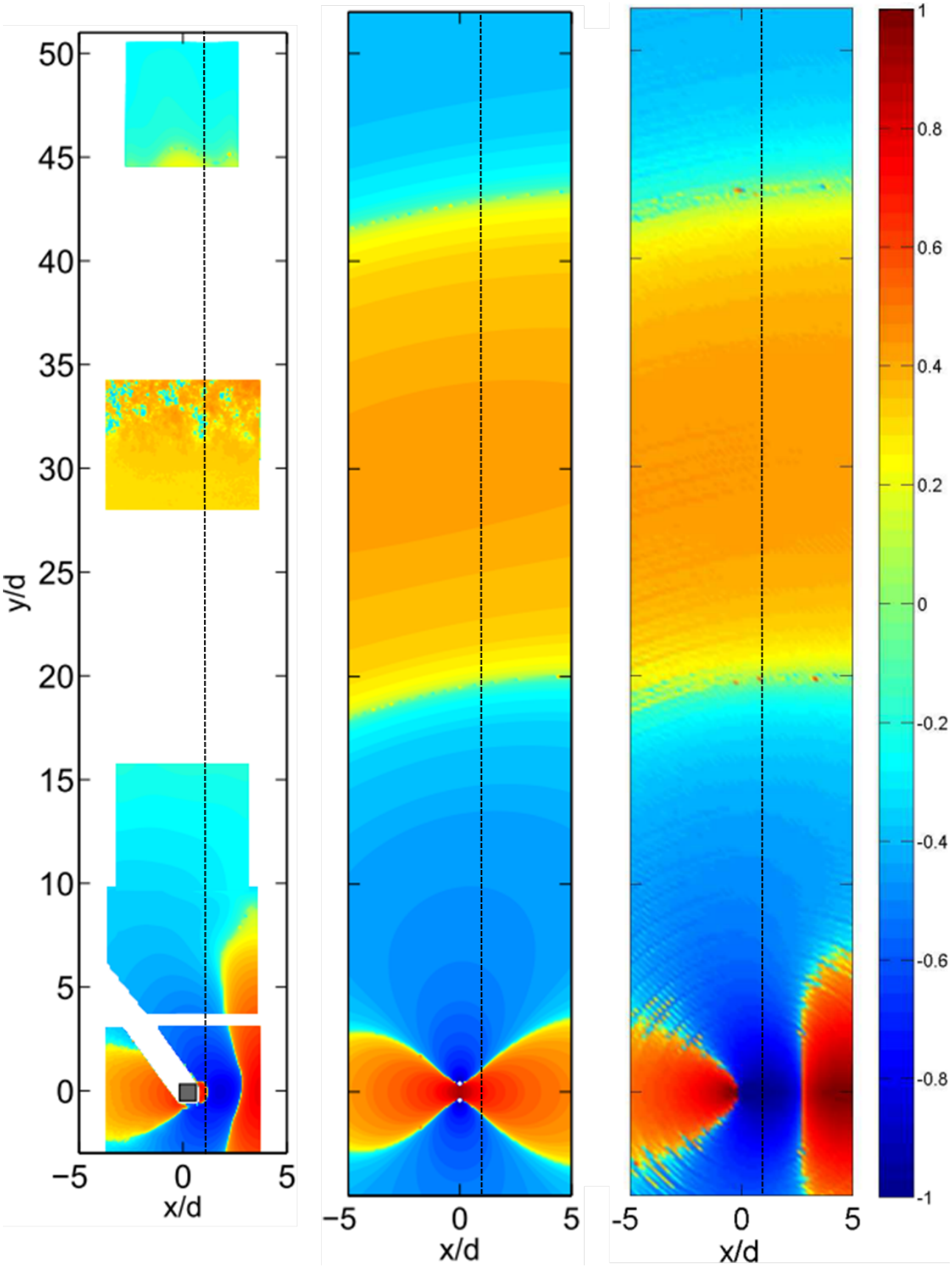

Figure 5: Snapshot of instantaneous distributions of the cross-correlation function (left), the analytical solution (middle) and the numerical simulation (right). The dashed lines indicate positions for further evaluations.

References

[1] Henning A, Kaepernick K, Ehrenfried K, Koop L, Dillmann A (2008) Investigation of aeroacoustic noise generation by simultaneous particle image velocimetry and microphone measurement. Experiments in Fluids Vol. 348:1073 – 1085

[2] Henning A, Koop L, Ehrenfried K (2010) Simultaneous multiplane piv and microphone array measurements on a rod-airfoil configuration. AIAA Journal 44(48):2263–2273

[3] Henning A, Koop L, Schroeder A (2013) Causality correlation analysis on a cold jet by means of simultaneous particle image velocimetry and microphone measurements. Journal of Sound and Vibration 332(13):3148 – 3162

[4] Iglesias E, Thompson D, Smith M (2016) Experimental study of the aerodynamic noise radiated by cylinders with different cross-sections and yaw angles. J Sound Vib 361:108–129

[5] Kähler C, Sammler B, Kompenhans J (2002) Generation and control of tracer particles for optical flow inverstigation in air. Experiments in Fluids 33:736–742

[6] Kähler CJ (2003) General design and operating rules for seeding atomisers. In: 5th International Symposium on Particle Image Velocimety, Busan, Korea, September 22-24

[7] Lee HK, Ribner HS (1972) Direct correlation of noise and flow of a jet. JASA 52(5):1280–1290

[8] Mueller TJ (ed) (2002) Aeroacoustic Measurements. Springer

[9] Norberg C (2003) Fluctuating lift on a circular cylinder: review and new measurements. Journal of Fluid Structures 17:57–96

[10] Pott-Pollenske M, Delfs J (2008) Enhanced capabilities of the aeroacoustic wind tunnel braunschweig. In: 14th AIAA/CEAS Aeroacoustics Conference, Vancouver, Canada., AIAA-2008-2910

[11] Raffel M, Willert CE, Wereley ST, Kompenhans J (2007) Particle Image Velocimetry - A Practical Guide, 2nd edn. Springer

[12] Ribner HS (1969) Quadrupole correlations governing the pattern of jet noise. J Fluid Mech 38(1):1–24

[13] Schaffar M (1979) Direct measurement of the correlation between axial in-jet velocity fluctuations and far field noise near the axis of a cold jet. J Sound Vib 64(1):73–83

[14] Treeby B, Cox B (2010) Matlab toolbox for the simulation and reconstruction of photoacoustic wave fields. J Biomed Opt 15(2)

[15] Treeby B, Jaros J, Rendell A, Cox B (2012) Modeling nonlinear ultrasound propagation in heterogeneous media with power law absorption using a k -space pseudospectral method. J Acoust Soc Am 131(6):432436

[16] Williamson C (1996) Vortex dynamics in the cylinder wake. Annual Reviews Fluid Mech 28:477–539

[17] Zdravkovich MM (1997) Flow Around Circular Cylinders, vol 1, 1st edn. Oxford science publications